

Moiré Exchange Effect in Twisted WSe₂/WS₂ Heterobilayer

Jiayi Zhu,^{1,‡} Huiyuan Zheng,^{2,‡} Xi Wang,^{1,3,4,‡} Heonjoon Park^{ⓧ,1}, Chengxin Xiao^{ⓧ,2}, Yinong Zhang^{ⓧ,1}, Takashi Taniguchi^{ⓧ,5}, Kenji Watanabe^{ⓧ,6}, Jiaqiang Yan^{ⓧ,7}, Daniel R. Gamelin^{ⓧ,8}, Wang Yao,^{2,9,*} and Xiaodong Xu^{ⓧ,1,10,†}

¹Department of Physics, University of Washington, Seattle, Washington, USA

²Department of Physics, University of Hong Kong, Hong Kong, China

³Department of Physics, Washington University, Saint Louis, Missouri 63130, USA

⁴Institute of Materials Science and Engineering, Washington University, St. Louis, Missouri 63130, USA

⁵Research Center for Materials Nanoarchitectonics, National Institute for Materials Science, 1-1 Namiki, Tsukuba 305-0044, Japan


⁶Research Center for Electronic and Optical Materials, National Institute for Materials Science, 1-1 Namiki, Tsukuba 305-0044, Japan

⁷Materials Science and Technology Division, Oak Ridge National Laboratory, Oak Ridge, Tennessee 37831, USA

⁸Department of Chemistry, University of Washington, Seattle, Washington, USA

⁹HKU-UCAS Joint Institute of Theoretical and Computational Physics at Hong Kong, China

¹⁰Department of Materials Science and Engineering, University of Washington, Seattle, Washington, USA

 (Received 27 March 2024; revised 21 June 2024; accepted 11 July 2024; published 21 August 2024)

Moiré superlattices of layered transition metal dichalcogenides are proven to host periodic electron crystals due to strong correlation effects. These electron crystals can also be intertwined with intricate magnetic phenomena. In this Letter, we present our findings on the moiré exchange effect, resulting from the modulation of local magnetic moments by electron crystals within well-aligned WSe₂/WS₂ heterobilayers. Employing polarization-resolved magneto-optical spectroscopy, we unveil a high-energy excitonic resonance near one hole per moiré unit cell ($\nu = -1$), which possesses a giant g factor several times greater than the already very large g factor of the WSe₂ A exciton in this heterostructure. Supported by continuum model calculations, these high-energy states are found to be dark excitons brightened through Umklapp scattering from the moiré mini-Brillouin zone. When the carriers form a Mott insulating state near $\nu = -1$, the Coulomb exchange between doped carriers and excitons forms an effective magnetic field with moiré periodicity. This moiré exchange effect gives rise to the observed giant g factor for the excitonic Umklapp state.

DOI: 10.1103/PhysRevLett.133.086501

Twisting two layers of two-dimensional materials results in the emergence of moiré superlattices characterized by periodic electronic potentials. Among these, moiré superlattices composed of transition metal dichalcogenides (TMDs) have attracted significant attention due to their potential for manipulating intricate electronic phases [1–3]. A diverse range of phases has been observed or predicted in these systems, including generalized Wigner crystals [4–12], Mott insulators [6,13,14], charge transfer insulators [15], bosonic (excitonic) insulators [8,16–20], and zero-field integer [21] and fractional Chern insulators [22–25]. In certain correlated states, nonmagnetic TMDs can exhibit local magnetic moments and magnetic ordering [26–32]. Prior investigations have demonstrated that the intricate magnetic couplings within TMD moiré superlattices are closely tied to electron-electron interactions [3,33]. The interplay between magnetism and electron correlation underscores that magnetism can be significantly influenced

by multiple factors, including the spatial separation between electrons, the order of layer stacking, and lattice configuration [2,34,35].

Another intriguing phenomenon associated with moiré superlattices is the Bragg-Umklapp scattering arising from the reciprocal lattice of the moiré supercell [36,37]. This scattering process effectively folds electronic states that originally reside in neighboring mini-Brillouin zones into the first mini-Brillouin zone. Notably, in TMD systems, which are known for their strong light-matter interactions and excitonic effects, Umklapp scattering leads to the emergence of new bright excitonic states. For instance, in the case of WSe₂/WS₂ heterobilayers subject to moiré superlattices, two distinct excitonic resonances appear at energies above the A exciton [36]. Similarly, in monolayer MoSe₂, a peak that blue shifts with increasing doping is observed at higher energy due to the formation of Wigner crystals, which is attributed to the effects of Umklapp scattering from the electron lattice [10].

Here, we report the observation of a giant Zeeman splitting of an Umklapp exciton in WSe₂/WS₂ with near 0° twist angle. At $\nu = -1$ (i.e., one hole per moiré site), it was proposed that a 120° Néel order can emerge as a result

*Contact author: wangyao@hku.hk

†Contact author: xuxd@uw.edu

‡These authors contributed equally to this work.

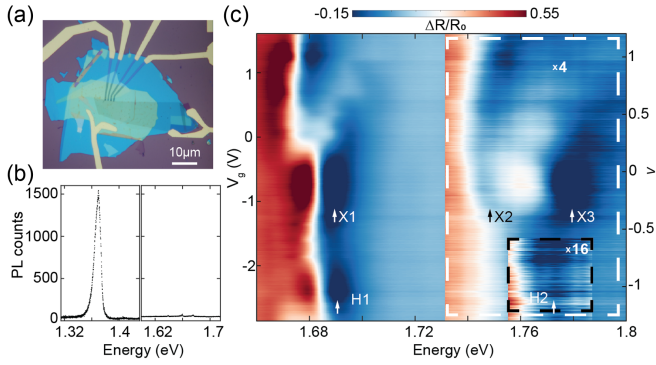


FIG. 1. Device basics and characterization. (a) Optical microscope image of device D1. (b) Photoluminescence spectrum of a representative R -stacked device. The left and right panels show interlayer and intralayer exciton photoluminescence, respectively. The intralayer exciton photoluminescence is strongly suppressed due to efficient charge transfer between the WSe_2 and WS_2 layers. (c) Reflectance contrast spectra of device D1 versus gate voltage and moiré filling factor at 5 K. X1, X2, and X3 denote the 1st, 2nd, and 3rd excitonic peaks at charge neutrality. H1 and H2 mark the exciton peaks at hole doping near filling factor -1 . The contrast reflectance intensity in high-energy spectral range (marked by the dashed box) is multiplied by 4 to magnify the weak features, and the inserted small window is magnified by 16 times.

of kinetic antiferromagnetic-exchange interactions between localized holes [14,33]. The interaction with this magnetic order is responsible for the observed large Zeeman splitting of the WSe_2 A exciton in such heterostructures [14]. In our study, we observe a giant Zeeman splitting for a higher energy state, with a g factor more than 5 times larger than that of the A exciton. This high-energy state is found to be a dark exciton brightened through Umklapp scattering from periodic moiré potential. Its Coulomb exchange with the external magnetic field polarized moiré carriers is responsible for the observed giant Zeeman splitting. The phenomenon is well captured by our model that incorporates moiré potential and a periodic moiré exchange field. The effect from a periodic magnetic field was previously proposed theoretically as “moiré Zeeman effect” [38].

We fabricated rhombohedral-stacked WSe_2/WS_2 heterostructures with near 0° alignment (see Methods for details). The sample is in dual gated geometry, which enables independent control of doping density and out-of-plane electric fields. The data are taken from two devices with moiré periodicities of approximately 8 nm (D1) and 8.5 nm (D2), corresponding to twist angles of 0.8° and 0.2° , respectively. The determination of moiré wavelengths is based on a combination of piezoresponse force microscopy, the doping-dependent photoluminescence (PL), and optical reflection measurements [Supplemental Material [39], Figs. S1 and S2(a)]. All measurements were conducted at a temperature of 1.6 K unless otherwise specified. Figure 1(a) displays an optical microscope image of device D1. We use strongly quenched intralayer exciton [right

panel in Fig. 1(b)] with the presence of a narrow interlayer exciton emission [left panel in Fig. 1(b)] to demonstrate high quality of the heterobilayer device.

Our investigations primarily focus on the reflectance contrast spectrum $(R - R_0)/R_0 = \Delta R/R_0$ in the vicinity of the WSe_2 resonances. Here, R and R_0 are reflectance measured on and off the heterostructure, respectively (details in Methods). In Fig. 1(c), we present the doping-dependent reflectance contrast of device D1, with the corresponding filling factors indicated. The filling factors are assigned based on a comparison between reflectance and PL spectra (details in Methods). Near charge neutrality, three intralayer moiré exciton features, labeled as X1, X2, and X3 in Fig. 1(c), are identified, which are consistent with previous results [36]. When the heterostructure is hole doped, X2 and X3 disappear. A new peak [labeled as H2 in Fig. 1(c)] emerges at about 80 meV above the ground state exciton H1 near $\nu = -1$. Notably, this peak is absent in monolayer WSe_2 [48]. We attribute peak H2 to Umklapp excitonic states arising from the moiré potential as well as a periodic effective magnetic field attached to moiré. While these high-energy states remain dark in monolayer systems, the periodic potential and the electron lattice introduce spatial modulation of the energy and wave function of the intralayer exciton. The brightening of Umklapp states can be understood from the perspective of momentum space. The initially dark states become coupled to the bright states at the Γ points through Umklapp scattering mediated by a moiré reciprocal lattice vector. When the periodicity of the exchange field is the same as that of the spin independent moiré potential, scatterings by these two potentials will form a bright Umklapp state in a constructive way. Consequently, these Umklapp states inherit the optical dipole of the bright states, rendering them optically active. As a result, the oscillator strength of peak H2 is significantly enhanced, making it observable in the reflectance spectra.

We performed circular polarization-resolved reflection measurements $\Delta R/R_0$ near $\nu = -1$. Figure 2(a) shows the spectra at selected magnetic fields applied in Faraday geometry. All magnetic field dependent data in the main text are from device D2 (see Figs. S3 and S4 [39] for D1). The dashed lines in Fig. 2(a) depict the evolution of both H1 and H2 peaks versus magnetic field, highlighting their significant field dependence. The extracted polarization-resolved peak positions (E) of H1 and H2 are shown in Figs. 2(b) and 2(c), respectively. To obtain the Zeeman splitting, we calculated the energy difference (Δ) between the right- (R) and left-handed (L) circularly polarized spectral peaks. As shown in Fig. 2(d), both peaks have pronounced Zeeman splittings, with $\Delta(\text{H2})$ being notably larger than $\Delta(\text{H1})$.

The enhancement of $\Delta(\text{H2})$ is particularly evident at $\nu = -1$, where the electron lattice is commensurate with the moiré superlattice. In contrast, the large Zeeman

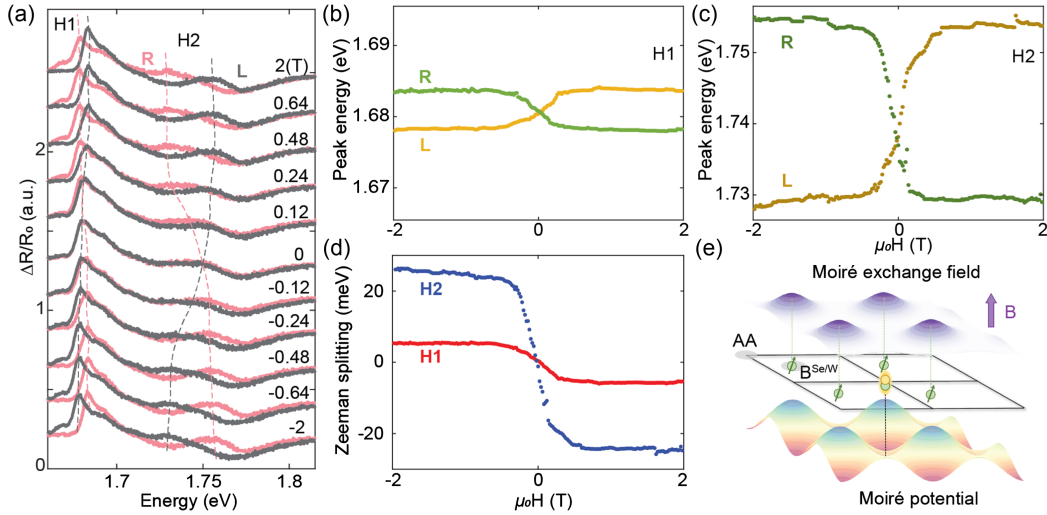


FIG. 2. Giant Zeeman splitting of Umklapp exciton state. Results are from device D2 at $\nu = -1$. (a) Circularly polarized reflectance contrast spectra at selected magnetic fields. Gray (pink) lines correspond to left-circular L (right-circular R) polarized spectra. Dashed lines trace the R and L polarized peak positions of H2. (b),(c) Extracted polarization resolved peak positions of H1 (b) and H2 (c) versus magnetic field. Green (yellow) dots in both panels correspond to peak energy extracted in R (L) polarized spectra. (d) Zeeman splitting of H1 (red) and H2 (blue) versus magnetic field at $\nu = -1$. H2 possesses a significantly larger splitting than H1. (e) Schematic of moiré excitons in moiré potential and moiré exchange field. Green (yellow) dots stand for holes (electrons). The location of the exciton and holes are shown in the moiré supercell. AA sites are minima of the moiré potential (bottom layer) and $B^{Se/W}$ sites are maxima of the moiré exchange field (upper layer).

splitting is absent in X2 and X3 at charge neutrality. This observation highlights the connection between local effective magnetic fields and the electron lattice. At $\nu = -1$, holes are localized at high symmetry $B^{Se/W}$ sites of the moiré superlattice, forming a triangular lattice [11,49]. When subjected to an external magnetic field, the hole spins align. The Umklapp states acquire optical dipole through scattering with bright states at the Γ point. The magnetic lattice enables these states to gain the large energy splitting of excitons in opposite valleys. Notably, the magnetic lattice shares the same periodicity as the moiré superlattice, as illustrated in Fig. 2(e). Consequently, the Umklapp scattering shares the same reciprocal lattice vectors as the magnetic lattice, which results in a significant contribution from the moiré exchange field to the Hamiltonian.

To further explain why Umklapp excitons exhibit a giant Zeeman splitting, we performed simulations of spin arrangements considering both the moiré potential and the periodic effective magnetic field, as depicted schematically in Fig. 2(e). The simulation of magnetization utilizes the periodic Gaussian wave packets. Our model follows the Refs. [11,49,50] for the assignment of exciton and hole positions. The moiré exchange field at r generated by the doped holes can be written as

$$M(\mathbf{r}) = M_0 \sum_{\mathbf{R}} e^{-(\mathbf{r}-\mathbf{R}-\mathbf{R}_{AB})^2/w^2}, \quad (1)$$

where M_0 denotes the strength of the exchange interaction between excitons and magnetized holes. \mathbf{R} is the moiré

lattice vector, and R_{AB} denotes the high symmetry point $B^{Se/W}$ of the supercell where holes reside. w is the wave packet width. We use the continuum model to describe the intralayer excitons from two opposite valleys. Pauli matrices σ are used to describe the valley degree of freedom. The Hamiltonian, described as follows in Eq. (2), consists of the pristine intralayer excitons and the moiré potential:

$$H = \left[\frac{\hat{p}^2}{2m} + V(\mathbf{r}) \right] I_2 + M(\mathbf{r}) \sigma_z. \quad (2)$$

On the right-hand side of Eq. (2), the first term denotes the kinetic energy of excitons. $V(\mathbf{r})$ represents moiré potential, whose minima locates at AA sites and shares the same periodic structure as $M(\mathbf{r})$. I_2 denotes the identity and the Pauli matrix σ_z describes the valley pseudospin. The periodic moiré potential couples the exciton plane wave component to the adjacent moiré reciprocal lattice vectors with the identical scattering strength on two valleys, whereas the moiré exchange field does so with inversed scattering strength. The giant Zeeman energy originates from the Coulomb exchange between a moiré exciton and its surrounding localized holes (Weiss exchange field). We noted that in experiments splittings of both peaks saturate with field fast at around 0.5 T, where the hole spins are aligned with external field already and exchange field stops increasing. We also verify the validity of the magnitude of moiré exchange field by calculating the Coulomb exchange between an exciton and a hole wave packet. More

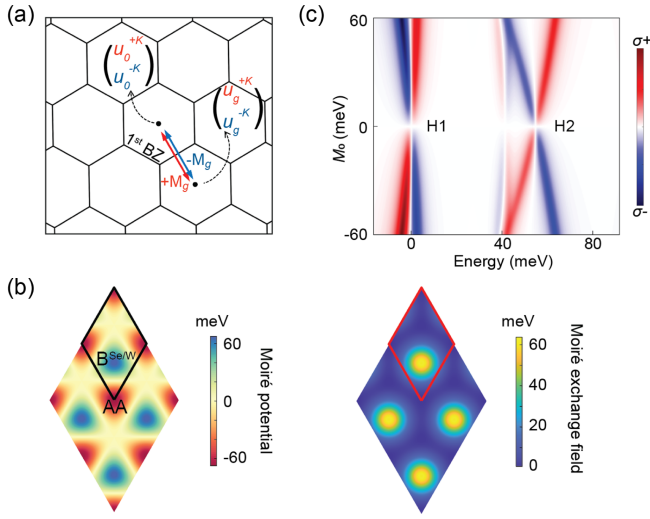


FIG. 3. Simulated excitonic scattering with moiré potential and moiré exchange field. (a) Schematics of exciton Umklapp scattering affected by moiré exchange field, where each state in momentum space consists of two valley components and they experience opposite scattering components. (b) Spatial maps of the moiré potential (left) and moiré exchange field (right) at saturation magnetic field. Red and black lines enclose one supercell. (c) Simulated polarization-resolved spectra with varying magnetic fields. The horizontal axis shows energy shifts from the zero-field ground exciton state, while the vertical axis represents the amplitude of moiré exchange field.

calculation details are elucidated in the Supplemental Material, Secs. S2 and S3 [39].

Figure 3(a) illustrates Umklapp scatterings with the presence of the moiré exchange field. Upon the activation of an external magnetic field, doped holes are magnetized, inducing an out-of-plane periodic exchange field. Excitons originating from opposite valleys experience reversed energy modulation due to this moiré exchange field. Consequently, Zeeman splitting appears at both ground and Umklapp states. As reported, the doped holes with spins mostly populate at $B^{\text{Se/W}}$ sites [11,49–51]; hence, the localized exchange field maximum is at $B^{\text{Se/W}}$ site as depicted in the left panel of Fig. 3(b). However, moiré potential to the exciton is shown to have minimum at AA sites [right panel in Fig. 3(b)], i.e., ground states are concentrated around AA sites [49,50]. Given the substantial reduction in the localized exchange field at AA sites [Fig. 3(b)], the Zeeman splitting on ground states is minor. On the other hand, the Umklapp states possess higher energy levels and more extended wave function (Fig. S7 in Supplemental Material, Sec. S2 [39]). Their density around AA sites contributes a minor Zeeman splitting while the extended density around $B^{\text{Se/W}}$ contributes the major Zeeman splitting. Based on this spatial overlap, Umklapp excitonic states would experience a stronger local exchange field than the ground state exciton. The simulation shows the Zeeman splitting of the exciton ground state and Umklapp

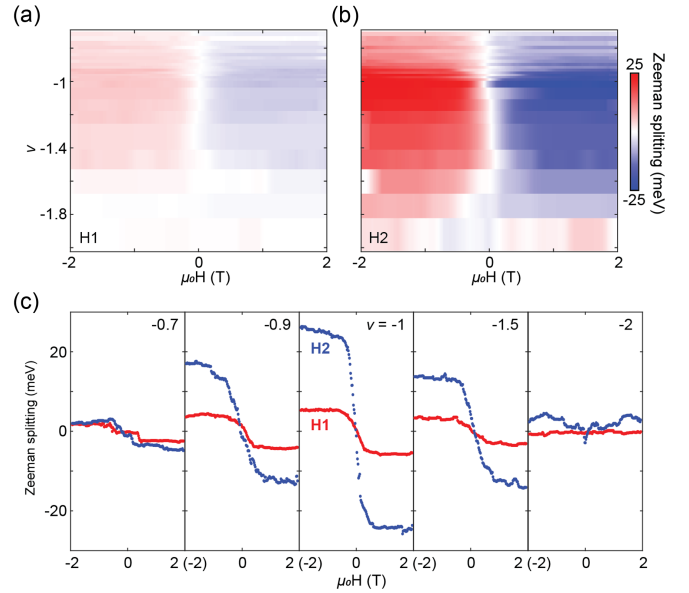


FIG. 4. Filling dependent Zeeman splitting. (a),(b) Zeeman splitting amplitude plots as a function of magnetic field and filling factor for peak H1 (a) and H2 (b). Both H1 and H2 exhibit maximum splitting near $\nu = -1$, with H2 exhibiting larger splitting across the entire filling factor range. (c) Linecuts of Zeeman splitting for H1 (red) and H2 (blue) at selected filling factors around $\nu = -1$.

state as a function of the exchange interaction strength [Fig. 3(c)], which agrees well with our experimental observation [Figs. 2(b) and 2(c)] when the amplitude of moiré exchange field is set comparable to moiré potential's amplitude. These simulation outcomes underscore the importance of periodic magnetism in moiré superlattices.

To confirm the significance of spins arising from electron lattices, we further measure the magnetic field dependence of $\Delta(\text{H1})$ [Fig. 4(a)] and $\Delta(\text{H2})$ [Fig. 4(b)] versus doping in the vicinity of $\nu = -1$. The linecuts with selective doping conditions are presented in Fig. 4(c) for a direct comparison. From these data, the effective g factors for H1 and H2 as a function of doping are extracted See Fig. S5 [39] as an example, when doping $\nu = -1$). Notably, when doped away from $\nu = -1$, the periodic exchange field weakens substantially. Both H1 and H2 experience reduced energy splitting. When the doping level is far from $\nu = -1$, the effective g factor of the ground state exciton is basically the same as the g factor in pristine monolayer WSe_2 [$\nu = -2$ in Fig. 4(c)]. It is noteworthy that, throughout the entire range of fillings investigated, H2 consistently displays a larger energy splitting than H1 (Fig. S6 [39]). In general, H2 originating from an Umklapp state is more sensitive to the moiré exchange effect than H1, and yields a sizable Zeeman splitting under the influence of the periodic magnetic background.

In summary, our work reports the observation of the moiré exchange effect. When the spins exhibit the same or commensurate periodicity as the one of excitons, Zeeman

splitting of the optical resonance is highly amplified on Umklapp scattered branches. These signatures can be potentially useful to investigate magnetic interactions in moiré lattices or moiré magnets [38]. In addition, the comparison of the Zeeman splitting of the Umklapp state to that of the ground state can provide information about wave-function distribution and potential profile in real space. Experiments also indicate the substantial influence of superlattice size and the real-space distribution of electron spins on the moiré exchange effect originating from the magnetic lattice. Furthermore, Umklapp state is facilitated by supercell reciprocal lattice vectors, making it potentially more sensitive to changes in moiré wavelength than the ground state. Since the TMD moiré superlattices rapidly emerge as a powerful platform for researching many-body interactions and topology, the insights gained in our work will help the community to further understand the emergent phenomena in moiré TMDs, such as those related to magneto-optical responses in the presence of mixed exciton-carriers.

Methods—Sample fabrication: The sample fabrication details can be found in Ref. [31]. In brief, a prefabricated bottom gate [a hexagonal boron nitride (hBN)—graphite stack] was transferred, and platinum contacts were made above the stack using conventional electron beam lithography methods. The bottom gate with contact was then cleaned by an atomic force microscope in contact mode. Mechanically exfoliated WS₂, WSe₂ monolayers were transferred using a flat polycarbonate (PC) and polydimethylsiloxane (PDMS) stamp onto the prefabricated and cleaned bottom gate. The crystal axis orientation of WS₂, WSe₂ was measured by linear polarization-resolved second harmonic generation. The twist angle was confirmed by piezoresponse force microscopy as mentioned elsewhere [31]. After the moiré wavelength was determined, the top graphite and hBN stack was transferred onto the bottom part for encapsulation and to realize the dual gate geometry.

Optical measurements: All optical measurements were conducted using a home-built confocal optical microscope in normal incident reflection geometry. The samples were cooled to 1.6 K using an exchange-gas cooled cryostat (attoDRY 2100) equipped with a 9 T superconducting magnet in Faraday configuration, and external magnetic fields were applied as necessary.

PL and reflection measurements were performed with the same supercontinuum laser, with and without the LLTF filter, and were dispersed by a diffraction grating (600 grooves per mm) and detected on a silicon CCD camera. The white light power used for reflection measurements was 15 nW for both devices. Reference spectra R₀ were taken at spots on the device but off of the WSe₂/WS₂ region. The PL was spectrally filtered from the laser using a long-pass filter before being directed into a spectrometer. The laser power used in PL measurements was 300 nW for

D1 and 40 nW for D2. The laser energy used in PL was in resonance with WSe₂ 1S state for the corresponding device.

Estimation of carrier density and filling factor: The carrier density is estimated using a parallel-plate capacitor model with the gate voltage applied. The BN thickness of samples was measured by atomic force microscope. D1 has around 37 nm top BN and 38 nm bottom BN. And the top and bottom BN thickness of D2 are 17 nm and 15 nm, respectively. The carrier density is calculated using $C_t\Delta V_t + C_b\Delta V_b$, where C_t (C_b) is the geometric capacitance of top (bottom) gate, and ΔV_t (ΔV_b) is the effective doping voltage (the relative voltage from band edge). The value used for the dielectric constant of BN is $\epsilon_{hBN} \approx 3$. The moiré wavelength is estimated through PFM measurements. Filling factor assignment involves a comprehensive analysis, including consideration of carrier density over moiré size and comparison of major features in gate dependent PL and reflectance contrast spectra (Supplemental Material, Figs. S1 and S2(a) [39]).

Acknowledgments—This work was mainly supported by DOE BES under Award No. DE-SC0018171. Sample fabrication and PFM characterization are partially supported by ARO MURI program (Grant No. W911NF-18-1-0431). The atomic force microscope-related measurements were performed using instrumentation supported by the U.S. National Science Foundation through the UW Molecular Engineering Materials Center (MEM-C), a Materials Research Science and Engineering Center (DMR-2308979). W. Y. acknowledges support by the Research Grants Council of Hong Kong SAR (AoE/P-701/20, HKU SRFS2122-7S05). Bulk WSe₂ crystal growth and characterization by J. Y. is supported by the US Department of Energy, Office of Science, Basic Energy Sciences, Materials Sciences and Engineering Division. K. W. and T. T. acknowledge support from the JSPS KAKENHI (Grants No. 20H00354 and No. 23H02052) and World Premier International Research Center Initiative (WPI), MEXT, Japan. X. X. acknowledges support from the State of Washington funded Clean Energy Institute and from the Boeing Distinguished Professorship in Physics.

Data availability—The datasets generated during and/or analyzed during this study are available from the contact author upon reasonable request.

X. X. and W. Y. conceived the project. X. W. and H. P. fabricated the samples. J. Z. performed the measurements, assisted by X. W. H. Z. and C. X. developed the model and performed the calculations. J. Z., H. Z., X. W., C. X., H. P., Y. Z., D. G., X. X., and W. Y. analyzed and interpreted the results. T. T. and K. W. synthesized the hBN crystals. J. Y. synthesized and characterized the bulk WSe₂ crystals. J. Z., H. Z., X. W., D. G., X. X., and W. Y. wrote the paper with input from all authors. All authors discussed the results.

The authors declare no competing financial interests.

- [1] K. Slagle and L. Fu, Charge transfer excitations, pair density waves, and superconductivity in moiré materials, *Phys. Rev. B* **102**, 235423 (2020).
- [2] N. C. Hu and A. H. MacDonald, Competing magnetic states in transition metal dichalcogenide moiré materials, *Phys. Rev. B* **104**, 214403 (2021).
- [3] F. Wu, T. Lovorn, E. Tutuc, and A. H. MacDonald, Hubbard model physics in transition metal dichalcogenide moiré bands, *Phys. Rev. Lett.* **121**, 026402 (2018).
- [4] Y. Zhou, J. Sung, E. Brutschea, I. Esterlis, Y. Wang, G. Scuri, R. J. Gelly, H. Heo, T. Taniguchi, and K. Watanabe *et al.*, Bilayer Wigner crystals in a transition metal dichalcogenide heterostructure, *Nature (London)* **595**, 48 (2021).
- [5] Y. Xu, S. Liu, D. A. Rhodes, K. Watanabe, T. Taniguchi, J. Hone, V. Elser, K. F. Mak, and J. Shan, Correlated insulating states at fractional fillings of moiré superlattices, *Nature (London)* **587**, 214 (2020).
- [6] E. C. Regan, D. Wang, C. Jin, M. I. B. Utama, B. Gao, X. Wei, S. Zhao, W. Zhao, Z. Zhang, and K. Yumigeta *et al.*, Mott and generalized Wigner crystal states in WSe_2/WSe_2 moiré superlattices, *Nature (London)* **579**, 359 (2020).
- [7] S. Miao, T. Wang, X. Huang, D. Chen, Z. Lian, C. Wang, M. Blei, T. Taniguchi, K. Watanabe, and S. Tongay *et al.*, Strong interaction between interlayer excitons and correlated electrons in WSe_2/WSe_2 moiré superlattice, *Nat. Commun.* **12**, 3608 (2021).
- [8] Z. Zhang, E. C. Regan, D. Wang, W. Zhao, S. Wang, M. Sayyad, K. Yumigeta, K. Watanabe, T. Taniguchi, S. Tongay *et al.*, Correlated interlayer exciton insulator in heterostructures of monolayer WSe_2 and moiré WS_2/WSe_2 , *Nat. Phys.* **18**, 1214 (2022).
- [9] X. Huang, T. Wang, S. Miao, C. Wang, Z. Li, Z. Lian, T. Taniguchi, K. Watanabe, S. Okamoto, and D. Xiao *et al.*, Correlated insulating states at fractional fillings of the WS_2/WSe_2 moiré lattice, *Nat. Phys.* **17**, 715 (2021).
- [10] T. Smoleński, P. E. Dolgirev, C. Kuhlenkamp, A. Popert, Y. Shimazaki, P. Back, X. Lu, M. Kroner, K. Watanabe, and T. Taniguchi *et al.*, Signatures of Wigner crystal of electrons in a monolayer semiconductor, *Nature (London)* **595**, 53 (2021).
- [11] H. Li, S. Li, E. C. Regan, D. Wang, W. Zhao, S. Kahn, K. Yumigeta, M. Blei, T. Taniguchi, and K. Watanabe *et al.*, Imaging two-dimensional generalized Wigner crystals, *Nature (London)* **597**, 650 (2021).
- [12] L. Wang, E. M. Shih, A. Ghiotto, L. Xian, D. A. Rhodes, C. Tan, M. Claassen, D. M. Kennes, Y. Bai, and B. Kim *et al.*, Correlated electronic phases in twisted bilayer transition metal dichalcogenides, *Nat. Mater.* **19**, 861 (2020).
- [13] Y. Tang, J. Gu, S. Liu, K. Watanabe, T. Taniguchi, J. C. Hone, K. F. Mak, and J. Shan, Dielectric catastrophe at the Wigner-Mott transition in a moiré superlattice, *Nat. Commun.* **13**, 4271 (2022).
- [14] Y. Tang, L. Li, T. Li, Y. Xu, S. Liu, K. Barmak, K. Watanabe, T. Taniguchi, A. H. MacDonald, and J. Shan *et al.*, Simulation of Hubbard model physics in WSe_2/WSe_2 moiré superlattices, *Nature (London)* **579**, 353 (2020).
- [15] Y. Zhang, N. F. Q. Yuan, and L. Fu, Moiré quantum chemistry: Charge transfer in transition metal dichalcogenide superlattices, *Phys. Rev. B* **102**, 201115 (2020).
- [16] Z. Lian, Y. Meng, L. Ma, I. Maity, L. Yan, Q. Wu, X. Huang, D. Chen, X. Chen, and X. Chen *et al.*, Valley-polarized excitonic Mott insulator in WS_2/WSe_2 moiré superlattice, *Nat. Phys.* **20**, 34 (2024).
- [17] H. Park, J. Zhu, X. Wang, Y. Wang, W. Holtzmann, T. Taniguchi, K. Watanabe, J. Yan, L. Fu, and T. Cao *et al.*, Dipole ladders with large Hubbard interaction in a moiré exciton lattice, *Nat. Phys.* **19**, 1286 (2023).
- [18] R. Xiong, J. H. Nie, S. L. Brantly, P. Hays, R. Sailus, K. Watanabe, T. Taniguchi, S. Tongay, and C. Jin, Correlated insulator of excitons in WSe_2/WS_2 moiré superlattices, *Science* **380**, 860 (2023).
- [19] L. Ma, P. X. Nguyen, Z. Wang, Y. Zeng, K. Watanabe, T. Taniguchi, A. H. MacDonald, K. F. Mak, and J. Shan, Strongly correlated excitonic insulator in atomic double layers, *Nature (London)* **598**, 585 (2021).
- [20] P. X. Nguyen, L. Ma, R. Chaturvedi, K. Watanabe, T. Taniguchi, J. Shan, and K. F. Mak, Perfect Coulomb drag in a dipolar excitonic insulator, [arXiv:2309.14940](https://arxiv.org/abs/2309.14940).
- [21] T. Li, S. Jiang, B. Shen, Y. Zhang, L. Li, Z. Tao, T. Devakul, K. Watanabe, T. Taniguchi, and L. Fu *et al.*, Quantum anomalous Hall effect from intertwined moiré bands, *Nature (London)* **600**, 641 (2021).
- [22] H. Park, J. Cai, E. Anderson, Y. Zhang, J. Zhu, X. Liu, C. Wang, W. Holtzmann, C. Hu, and Z. Liu *et al.*, Observation of fractionally quantized anomalous Hall effect, *Nature (London)* **622**, 74 (2023).
- [23] J. Cai, E. Anderson, C. Wang, X. Zhang, X. Liu, W. Holtzmann, Y. Zhang, F. Fan, T. Taniguchi, and K. Watanabe *et al.*, Signatures of fractional quantum anomalous Hall states in twisted $MoTe_2$, *Nature (London)* **622**, 63 (2023).
- [24] F. Xu, Z. Sun, T. Jia, C. Liu, C. Xu, C. Li, Y. Gu, K. Watanabe, T. Taniguchi, and B. Tong *et al.*, Observation of integer and fractional quantum anomalous Hall effects in twisted bilayer $MoTe_2$, *Phys. Rev. X* **13**, 031037 (2023).
- [25] Y. Zeng, Z. Xia, K. Kang, J. Zhu, P. Knüppel, C. Vaswani, K. Watanabe, T. Taniguchi, K. F. Mak, and J. Shan, Thermodynamic evidence of fractional Chern insulator in moiré $MoTe_2$, *Nature (London)* **622**, 69 (2023).
- [26] L. Ciorciaro, T. Smoleński, I. Morera, N. Kiper, S. Hiestand, M. Kroner, Y. Zhang, K. Watanabe, T. Taniguchi, and E. Demler *et al.*, Kinetic magnetism in triangular moiré materials, *Nature (London)* **623**, 509 (2023).
- [27] Y. Tang, K. Su, L. Li, Y. Xu, S. Liu, K. Watanabe, T. Taniguchi, J. Hone, C.-M. Jian, and C. Xu *et al.*, Evidence of frustrated magnetic interactions in a Wigner-Mott insulator, *Nat. Nanotechnol.* **18**, 233 (2023).
- [28] B. A. Foutty, J. Yu, T. Devakul, C. R. Kometter, Y. Zhang, K. Watanabe, T. Taniguchi, L. Fu, and B. E. Feldman, Tunable spin and valley excitations of correlated insulators in Γ -valley moiré bands, *Nat. Mater.* **22**, 731 (2023).
- [29] A. J. Campbell, M. Brotons-Gisbert, H. Baek, V. Vitale, T. Taniguchi, K. Watanabe, J. Lischner, and B. D. Gerardot, Exciton-polarons in the presence of strongly correlated electronic states in a $MoSe_2/WSe_2$ moiré superlattice, *npj 2D Mater. Appl.* **6**, 79 (2022).
- [30] E. Anderson, F.-R. Fan, J. Cai, W. Holtzmann, T. Taniguchi, K. Watanabe, D. Xiao, W. Yao, and X. Xu, Programming

- correlated magnetic states with gate-controlled moiré geometry, *Science* **381**, 325 (2023).
- [31] X. Wang, C. Xiao, H. Park, J. Zhu, C. Wang, T. Taniguchi, K. Watanabe, J. Yan, D. Xiao, and D. R. Gamelin *et al.*, Light-induced ferromagnetism in moiré superlattices, *Nature (London)* **604**, 468 (2022).
- [32] Z. Tao, B. Shen, W. Zhao, N. C. Hu, T. Li, S. Jiang, L. Li, K. Watanabe, T. Taniguchi, and A. H. MacDonald *et al.*, Giant spin Hall effect in AB-stacked MoTe₂/WSe₂ bilayers, arXiv:2303.12881.
- [33] T. Devakul, V. Crépel, Y. Zhang, and L. Fu, Magic in twisted transition metal dichalcogenide bilayers, *Nat. Commun.* **12**, 6730 (2021).
- [34] M. Davydova, Y. Zhang, and L. Fu, Itinerant spin polaron and metallic ferromagnetism in semiconductor moiré superlattices, *Phys. Rev. B* **107**, 224420 (2023).
- [35] N. Morales-Durán, P. Potasz, and A. H. Macdonald, Magnetism and quantum melting in moiré-material Wigner crystals, *Phys. Rev. B* **107**, 235131 (2023).
- [36] C. Jin, E. C. Regan, A. Yan, M. I. B. Utama, D. Wang, S. Zhao, Y. Qin, S. Yang, Z. Zheng, and S. Shi *et al.*, Observation of moiré excitons in WSe₂/WS₂ heterostructure superlattices, *Nature (London)* **567**, 76 (2019).
- [37] Y. Shimazaki, C. Kuhlenkamp, I. Schwartz, T. Smoleński, K. Watanabe, T. Taniguchi, M. Kroner, R. Schmidt, M. Knap, and A. İmamoğlu, Optical signatures of periodic charge distribution in a Mott-like correlated insulator state, *Phys. Rev. X* **11**, 021027 (2021).
- [38] A. G. Salvador, C. Kuhlenkamp, L. Ciorciaro, M. Knap, and A. İmamoğlu, Optical signatures of periodic magnetization: The moiré Zeeman effect, *Phys. Rev. Lett.* **128**, 237401 (2022).
- [39] See Supplemental Material at <http://link.aps.org/supplemental/10.1103/PhysRevLett.133.086501> for additional information and data from the repeat device and a detailed discussion of the theory and calculations, which includes Refs. [41–48].
- [40] H. Yu, G.-B. Liu, J. Tang, X. Xu, and W. Yao, Moiré excitons: From programmable quantum emitter arrays to spin-orbit-coupled artificial lattices, *Sci. Adv.* **3**, e1701696 (2017).
- [41] D. Y. Qiu, T. Cao, and S. G. Louie, Nonanalyticity, valley quantum phases, and lightlike exciton dispersion in monolayer transition metal dichalcogenides: Theory and first-principles calculations, *Phys. Rev. Lett.* **115**, 176801 (2015).
- [42] P. L. Altick and A. E. Glassgold, Correlation effects in atomic structure using the random-phase approximation, *Phys. Rev.* **133**, A632 (1964).
- [43] A. Torche and G. Bester, First-principles many-body theory for charged and neutral excitations: Trion fine structure splitting in transition metal dichalcogenides, *Phys. Rev. B* **100**, 201403 (2019).
- [44] M. Combescot, O. Betbeder-Matibet, and F. Dubin, The many-body physics of composite bosons, *Phys. Rep.* **463**, 215 (2008).
- [45] S. Y. Shiau, M. Combescot, and Y. C. Chang, Trion ground state, excited states, and absorption spectrum using electron-exciton basis, *Phys. Rev. B—Condens. Matter Mater. Phys.* **86**, 115210 (2012).
- [46] M. Danovich, D. A. Ruiz-Tijerina, R. J. Hunt, M. Szymszowski, N. D. Drummond, and V. I. Fal’ko, Localized interlayer complexes in heterobilayer transition metal dichalcogenides, *Phys. Rev. B* **97**, 195452 (2018).
- [47] D. A. Ruiz-Tijerina, I. Soltero, and F. Mireles, Theory of moiré localized excitons in transition metal dichalcogenide heterobilayers, *Phys. Rev. B* **102**, 195403 (2020).
- [48] T. Wang, Z. Li, Z. Lu, Y. Li, S. Miao, Z. Lian, Y. Meng, M. Blei, T. Taniguchi, and K. Watanabe *et al.*, Observation of quantized exciton energies in monolayer WSe₂ under a strong magnetic field, *Phys. Rev. X* **10**, 021024 (2020).
- [49] M. H. Naik, E. C. Regan, Z. Zhang, Y.-H. Chan, Z. Li, D. Wang, Y. Yoon, C. S. Ong, W. Zhao, and S. Zhao *et al.*, Intralayer charge-transfer moiré excitons in van der Waals superlattices, *Nature (London)* **609**, 52 (2022).
- [50] S. Susarla, M. H. Naik, D. D. Blach, J. Zipfel, T. Taniguchi, K. Watanabe, L. Huang, R. Ramesh, F. H. D. Jornada, and S. G. Louie *et al.*, Hyperspectral imaging of exciton confinement within a moiré unit cell with a subnanometer electron probe, *Science* **378**, 1235 (2022).
- [51] X. Wang, X. Zhang, J. Zhu, H. Park, Y. Wang, C. Wang, W. G. Holtzmann, T. Taniguchi, K. Watanabe, and J. Yan *et al.*, Intercell moiré exciton complexes in electron lattices, *Nat. Mater.* **22**, 599 (2023).